



# Can root systems redistribute soil water to mitigate the effects of drought?

Andrew Mair<sup>a,\*</sup>, Lionel Dupuy<sup>b</sup>, Mariya Ptashnyk<sup>c</sup>

<sup>a</sup> The Maxwell Institute for Mathematical Sciences, The Bayes Centre, 47 Potterrow, Edinburgh EH8 9BT, Scotland, UK

<sup>b</sup> Department of Conservation of Natural Resources, Neiker & IKERBASQUE, Basque Foundation for Science, Bilbao, Spain

<sup>c</sup> School of Mathematical and Computer Sciences, Heriot-Watt University, The Maxwell Institute for Mathematical Sciences, Edinburgh, Scotland, UK

## ARTICLE INFO

### Keywords:

Drought resistance  
Water lifetime  
Preferential flow  
Root architecture  
Richards equation

## ABSTRACT

**Context:** Plants combine a diverse range of well-studied morphological and physiological mechanisms to adapt to water deficit and drought. In addition to this, plant roots have also been shown to induce preferential flows of water through vegetated soil. However, less is known about the contribution of this particular phenomenon to a plant's capacity to resist drought.

**Objective:** This work investigates how root-induced preferential flow redistributes soil water according to the architecture of a root system and how this may influence plant drought resistance. Specifically, we consider how this redistribution of soil water affects the length of time that water remains in the rooted zone and available for uptake following a precipitation event.

**Methods:** We developed a model for water transport through vegetated soil that incorporates root-induced preferential flow, and then used Bayesian optimisation to calibrate the model against experimental data. A finite element scheme was used to simulate the model and assess how the fate of soil water is impacted by preferential flow strength, soil type, and root system architecture.

**Results:** As the preferential flow strength induced by a root system was increased, evaporation from the soil surface reduced, but deep percolation from the rooted zone increased. When assessing the effect of root architecture, it was found that a root system with reduced gravitropic response retained the most water in the soil around its roots over a 7-day post-precipitation period.

**Conclusion:** Our findings indicate that an optimal preferential flow strength exists for minimising water loss from the rooted zone and that this optimum differs with soil type. Furthermore, in instances where crops are rain fed or irrigated from above, results suggest that a reduction in gravitropic response allows a root system to uptake more of the water that enters the soil.

**Implications:** New insights are provided into the role of root system traits in plant drought resistance and root system architectures are identified for improved water use efficiency within cropping systems.

## 1. Introduction

Drought resistance in crops is due to the ability of plants to avoid dehydration through morphological and physiological mechanisms (Fang and Xiong, 2015). Primary responses usually involve adapting the processes that govern transpiration. For example, plant species regulate the opening and closure of their stomata in order to adjust levels of water loss via transpiration (Luo, 2010). Leaves can also produce waxes (Goodwin and Jenks, 2005) and roll (Cal et al., 2019) to reduce permeability and transpiration area respectively.

A number of physiological root characteristics have been linked to improved drought resistance. The development of the root exodermis,

by the laying down of Casparian bands and suberin lamellae, improves water retention by reducing the radial hydraulic conductivity of root tissue (Frensch and Steudle, 1989; Taleisnik et al., 1999; Hose et al., 2001). Plants can also increase solute concentration in their root cells, thus enabling water extraction at lower soil water potentials (Li et al., 2008).

Plant root activity also has a profound impact on the hydraulics of vegetated soil. The exudation of mucilage by roots has been shown to increase the water repellency of rhizosphere soil (Ahmed et al., 2016; Naveed et al., 2018) while, at the same time, roots produce surfactants (Read et al., 2003) that can reduce the surface tension of exudate solutions (Naveed et al., 2019) and aid water infiltration into dry soils

\* Corresponding author.

E-mail address: [adm13@hw.ac.uk](mailto:adm13@hw.ac.uk) (A. Mair).

<https://doi.org/10.1016/j.fcr.2023.109006>

Received 25 October 2022; Received in revised form 28 April 2023; Accepted 11 June 2023

Available online 20 June 2023

0378-4290/© 2023 The Author(s). Published by Elsevier B.V. This is an open access article under the CC BY license (<http://creativecommons.org/licenses/by/4.0/>).

(Stroosnijder et al., 2012; Lowe et al., 2017). Furthermore, there is substantial evidence that root activity alters the pore structure of soil. Previous studies have indicated that growing roots compress nearby soil particles as they expand and reduce soil porosity near their surface (Dexter, 1987; Bruand et al., 1996). However, other experimental results have revealed that root growth and the activity of the root microbiome actually lead to an increase in the porosity of surrounding soil (Feeney et al., 2006; Koebernick et al., 2019; Anselmucci et al., 2021). Overall, the combination of these modifications to soil properties has been found to manifest as an increase in the transport of soil water into directions that follow the orientation of roots (Noguchi et al., 1997; Michot et al., 2003; Lange et al., 2009; Beff et al., 2013). This is defined as preferential flow (Ghestem et al., 2011) and is likely to influence the fate of water that enters vegetated soil.

Since roots facilitate the flow of soil water in this way, then their architecture must strongly influence the availability of water to the plant. Numerous experimental investigations have been conducted to identify optimal architectures for drought resistance (Nepstad et al., 1994; Snyman, 2006; Lopes and Reynolds, 2010; Liu et al., 2013; Uga et al., 2013; Xu et al., 2017). In addition, various modelling and simulation-based approaches have previously been employed to study the effect of root system architecture on root water uptake. For example, Manschadi et al. (Manschadi et al., 2006) employed the cropping system model APSIM (Keating et al., 2003) to predict the yield of wheat and barley genotypes, with different root system properties, in various scenarios of initial stored soil water and in-crop rainfall.

There is also a long history of root architectural models being used in conjunction with soil water transport models to study the influence of root architecture on water uptake. Clausnitzer and Hopmans (1994) coupled a root architecture model of Pages et al. (1989) with Richards equation (Richards, 1931) to examine the spatial distribution of root water uptake. Somma et al. (1998) then extended this model by coupling it with a convection diffusion equation for solute transport. Doussan et al. (2006) again used these models, together with the hydraulic tree model (Doussan et al., 1998), to investigate the water uptake of fibrous and tap-rooted lupin root systems. This modelling strategy of parametrising Richards equation with a sink term that incorporates root tissue water transport was also developed by Javaux et al. (2008) and defined as an R-SWMS model. Both Draye et al. (2010) and Leitner et al. (2014) have since used the R-SWMS model with more recent root architectural models, RootTyp (Pages et al., 2004) and RootBox (Leitner et al., 2010a), to assess root water uptake performance of Ryegrass and Maize root systems of contrasting architecture. A similar approach was also used by Schneider et al. (2010) but with a stand alone uptake term named aRoot. More recently, Koch et al. (2019) have applied magnetic resonance imaging data for root system architectures, along with dye-tracer observations of water infiltration patterns, in order to calibrate the root water uptake dynamics of an R-SWMS model.

However, these past studies all focus on how root architecture impacts a plant's ability to access water, whilst overlooking the preferential flow patterns induced by root architectures and how these influence the availability of water to the root system over time. Prior to canopy closure, evaporation from the soil surface is a major source of water loss from vegetated soil (Schwinning and Sala, 2004). Nevertheless, the leaching of water into soil layers below the root profile, referred to as deep percolation, and surface runoff, where precipitation fails to infiltrate into bulk soil due to the surface already being fully saturated, also contribute to total water loss (Bethune et al., 2008). These factors all combine to reduce the amount of water that is available for uptake by the plant and are bound to be affected by the preferential flow that is induced by a particular root system architecture.

A common approach for incorporating preferential flow into soil water transport simulations is to use a dual-porosity model. This approach involves two parametrisations of Richards equation, one that reflects the hydraulic characteristics of the preferential flow domain and another for the bulk soil. The two equations are then coupled by a water

exchange term (Gerke and Van Genuchten, 1993). When determining the preferential flow domain, dual-porosity models either assume a homogenous distribution of roots in the soil (Shao et al., 2017) or do not consider their distribution at all. Because of these limitations, there is an opportunity for new mathematical models that incorporate the influence of root architecture on preferential flow patterns and, hence, allow more complete assessment of the merits of specific root architectures in terms of improving a plant's capacity to resist drought.

This work aims to investigate how the architecture of a root system influences the way that soil water is redistributed following precipitation. The directions of water transport in the soil not only determine the availability of water for uptake by roots. They also affect the rate at which water is lost from the rooted soil layer. We therefore hypothesise that root system architecture can affect the post-precipitation water lifetime, which is the length of time that water remains available for plant uptake following precipitation (Fig. 1). We propose a model for water transport through vegetated soil, which combines root system architecture, root water uptake, and root-oriented preferential flow (Mair et al., 2022). Our model was calibrated for Maize plants with respect to experimental data on the hydraulic conductivity of soil vegetated by Maize (Feki et al., 2018). Simulations were performed to investigate the effect of root-oriented preferential flow on evaporation, deep percolation, and root water uptake. We examined how the architecture of a root system affected the time at which a water deficit occurred and, hence, proposed ideotypes for improved drought resistance.

## 2. Materials and methods

### 2.1. A model for soil water transport incorporating root water uptake and preferential flow

This work considers a root-soil system of a 3D domain of unsaturated soil  $\Omega$  occupied by a root system  $\mathfrak{R} \subset \Omega$ . Our model for water transport in the vegetated soil incorporates the influence of root system architecture by using density functions, which give continuous approximations of root abundance and orientation within the soil. The root system is defined as a finite union of  $N_{\mathfrak{R}}$  disjoint segments  $\mathfrak{R}_i$ , i.e.  $\mathfrak{R} = \sum_{i=1}^{N_{\mathfrak{R}}} \mathfrak{R}_i$ . Each root segment is defined by values for the positions and radii of its base and tip. Such data is obtained for real root systems through excavation and digitisation (Danjon et al., 1999) or the use of x-ray computed tomography (Zhao et al., 2020). It is also the typical output of root system architecture simulation platforms such as CRootBox (Schnepf et al., 2018) and OpenSimRoot (Postma et al., 2017). In this work the software CRootBox is used. This program employs an L-system model (Leitner et al., 2010b) to create virtual root system architectures from parameters such as root length, inter-lateral distance, and gravitropism. Here, the term gravitropism refers to the differential growth of roots, into downward directions, which occurs in response to the force of gravity.

Using the methods in Mair et al. (2022), we derive, from architecture data of a root system, the volumetric root density  $\psi$  ( $L^3L^{-3}$ ) and the root length density  $RLD$  ( $LL^{-3}$ ). In short, for a spatial co-ordinate  $x = (x_1, x_2, x_3)$  in the soil  $\Omega$ , the value of  $\psi(x) \in (0, 1)$  increases with root volume and the value of  $RLD(x)$  increases with root length. Furthermore,  $\psi$  and  $RLD$  integrate over the vegetated domain to give the total volume and root length of the root system respectively. Root-oriented preferential flow is incorporated into the model for water transport by  $\psi$ , and  $RLD$  is used to model root water uptake.

To model the influence of root architecture and abundance on the transport of water through soil, we use the PF model, recently developed in Mair et al. (2022):

$$\partial_t((1-\psi(x))\theta(h)) + \nabla \cdot ((1-\psi(x))\tilde{\mathbf{q}}) = -(1-\psi(x))S(x, t) \text{ in } \Omega \times (0, T]. \quad (1)$$

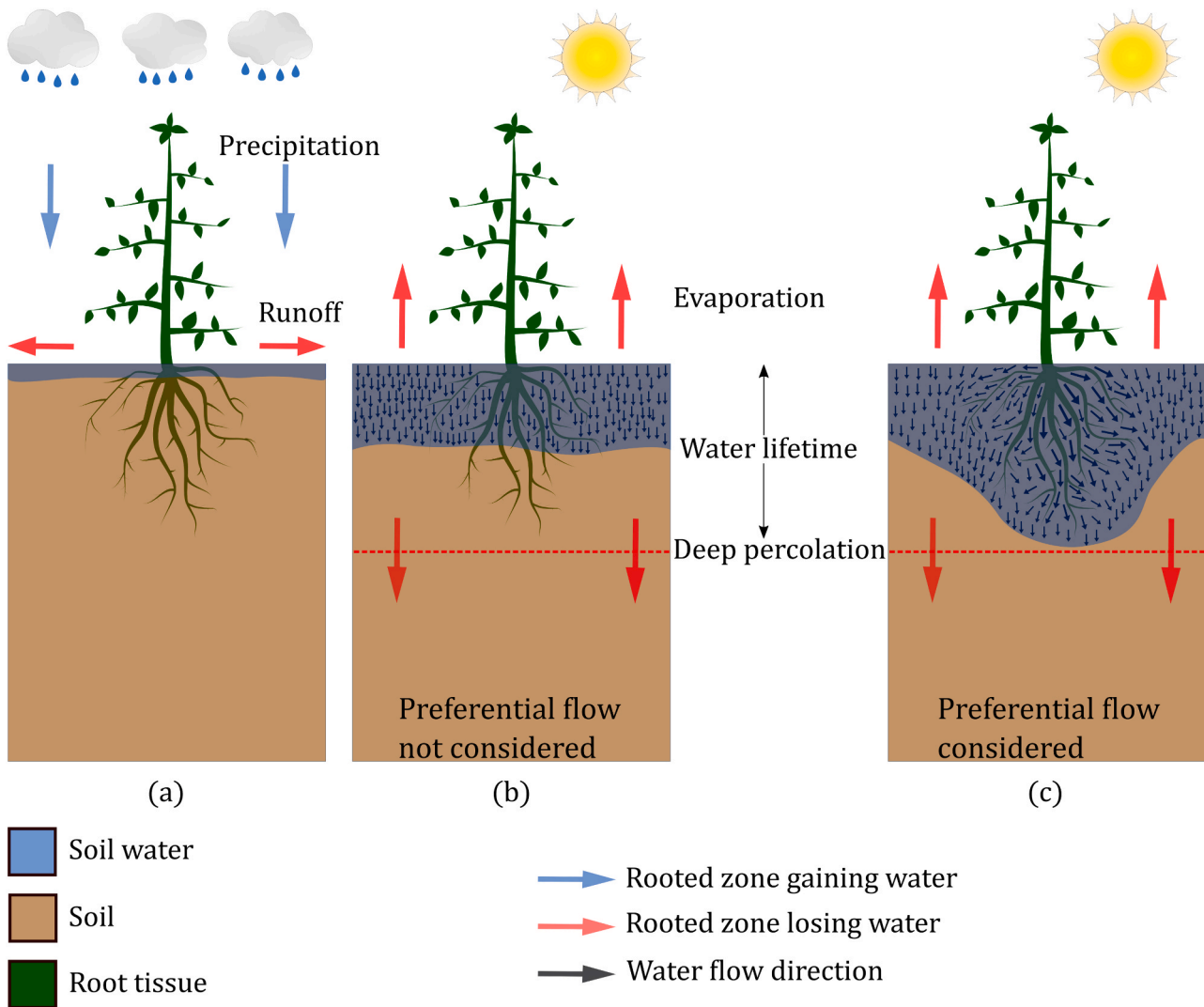


**Fig. 1.** Preferential flow and drought resistance. Drought occurs when a water deficit is maintained for sufficiently long enough for plant dehydration to occur. Following precipitation (a), if root-induced preferential flow is not considered (b), then the transport of soil water will not be affected by the root architecture. However, if preferential flow is considered (c), then soil water will be redistributed according to the architecture of the root system. The spatial distribution of water then affects evaporation and deep percolation rates, which in turn affects the duration of any water deficit imposed on the plant.

This is a modification of Richards equation (Richards, 1931), the classic model for the evolution of water content  $\theta$  ( $L^3L^{-3}$ ) within unsaturated soil, and is defined over a domain  $\Omega \subset \mathbb{R}^3$  with final time  $T > 0$ . The PF model (Eq. (1)) is solved for pressure head  $h$  (L). Root water uptake is accounted for by the sink term  $S$  ( $T^{-1}$ ), and, to incorporate the phenomena of root-oriented preferential flow, the water flux used in Eq. (1) has the following form:

$$\tilde{\mathbf{q}} = (1 - \psi)\mathbf{q} + H\mathbf{q}. \quad (2)$$

Here,  $\mathbf{q}$  ( $LT^{-1}$ ) is the isotropic flux for water flow through fallow unsaturated soil. Root-oriented preferential flow is accounted for in Eq. (2) by the flow-anisotropy matrix  $H$ , which is parametrised by the facilitation constant  $c_a > 1$  to determine the strength of the preferential flow induced. At a point  $x$  in the soil domain  $\Omega$ , left multiplication of the flux vector  $\mathbf{q}$  by  $H$ , increases the magnitude of  $\mathbf{q}$  in directions parallel to root segments in the near vicinity of  $x$ . This increase in magnitude is by a factor of  $c_a$  and scaled according to the value of local root volumetric density  $\psi(x)$ . Therefore, because  $c_a$  is fixed and  $\psi$  is bounded, we have that  $H$  is also bounded. Due to this formulation of  $H$ , it follows that in soil regions with low root abundance the first term in  $\tilde{\mathbf{q}}$  dominates and the flux closely resembles  $\mathbf{q}$ . However, in regions of soil close to roots the

second term in  $\tilde{\mathbf{q}}$  dominates and the flow of soil water is facilitated in directions parallel to root axes. An explicit mathematical formulation for  $H$  can be found in Mair et al. (2022).

The isotropic flux of water through fallow unsaturated soil is modelled using the law of Darcy (1856), Buckingham (1907):

$$\mathbf{q} = -K_s \kappa(h) \nabla(h + x_3). \quad (3)$$

Here, the soil's saturated hydraulic conductivity is given by the constant  $K_s$  ( $LT^{-1}$ ), and the relation between hydraulic conductivity and pressure head  $h$  is described by the function  $\kappa$ , which is defined using the classic model of Van Genuchten (1980) and Mualem (1976):

$$\theta(h) = \theta_r + \frac{\theta_s - \theta_r}{(1 + |\alpha_{vg} h|^n)^m}, \quad (4)$$

$$\kappa(h) = \left( \frac{\theta(h) - \theta_r}{\theta_s - \theta_r} \right)' \left[ 1 - \left( 1 - \left( \frac{\theta(h) - \theta_r}{\theta_s - \theta_r} \right)^{\frac{1}{m}} \right)^m \right]^2. \quad (5)$$

Parameter values in Eqs. (4) and (5) depend upon soil type. The residual and saturated water contents are given by  $\theta_r$  and  $\theta_s$  ( $L^3L^{-3}$ ) respectively, and  $\alpha_{vg}(L^{-1})$ ,  $n$  and  $m = 1 - 1/n$  are shape parameters, with  $n$  and  $m$

being dimensionless. The parameter  $l$  denotes the tortuosity.

Root water uptake is incorporated into the PF model (Eq. (1)) through the macroscopic sink term  $S$ , employed previously by Simunek and Hopmans (2009), which links soil water pressure head, normalised root length density  $NRLD$  ( $L^{-3}$ ), and potential plant transpiration  $\mathcal{T}_p$  ( $LT^{-1}$ ):

$$S(x, t) = \alpha_F(h) NRLD(x) A_{\mathcal{T}} \mathcal{T}_p \frac{1}{\max(\omega(t), \omega_c)}. \quad (6)$$

Here,  $0 \leq \alpha_F \leq 1$  is a dimensionless water stress response function that accounts for the impact of reduced water availability on root water uptake (Feddes, 1982). A dependence of root water uptake on the

distribution of roots within the soil is incorporated into  $S$  through the normalised root length density function:

$$NRLD(x) = \frac{RLD(x)}{\int_{\Omega} RLD(x) dx}. \quad (7)$$

The soil surface area associated with transpiration is denoted as  $A_{\mathcal{T}}$  ( $L^2$ ), and the dimensionless function  $\omega(t)$  is a measure of the global water stress experienced by the plant at a given time (Cai et al., 2018). The value of the critical water stress index  $\omega_c \in (0, 1)$  reflects the plant's capacity to compensate for low water availability in certain regions of vegetated soil by increasing uptake in wetter regions.

In this work the soil domain  $\Omega$  is assumed to be cuboidal. The upper

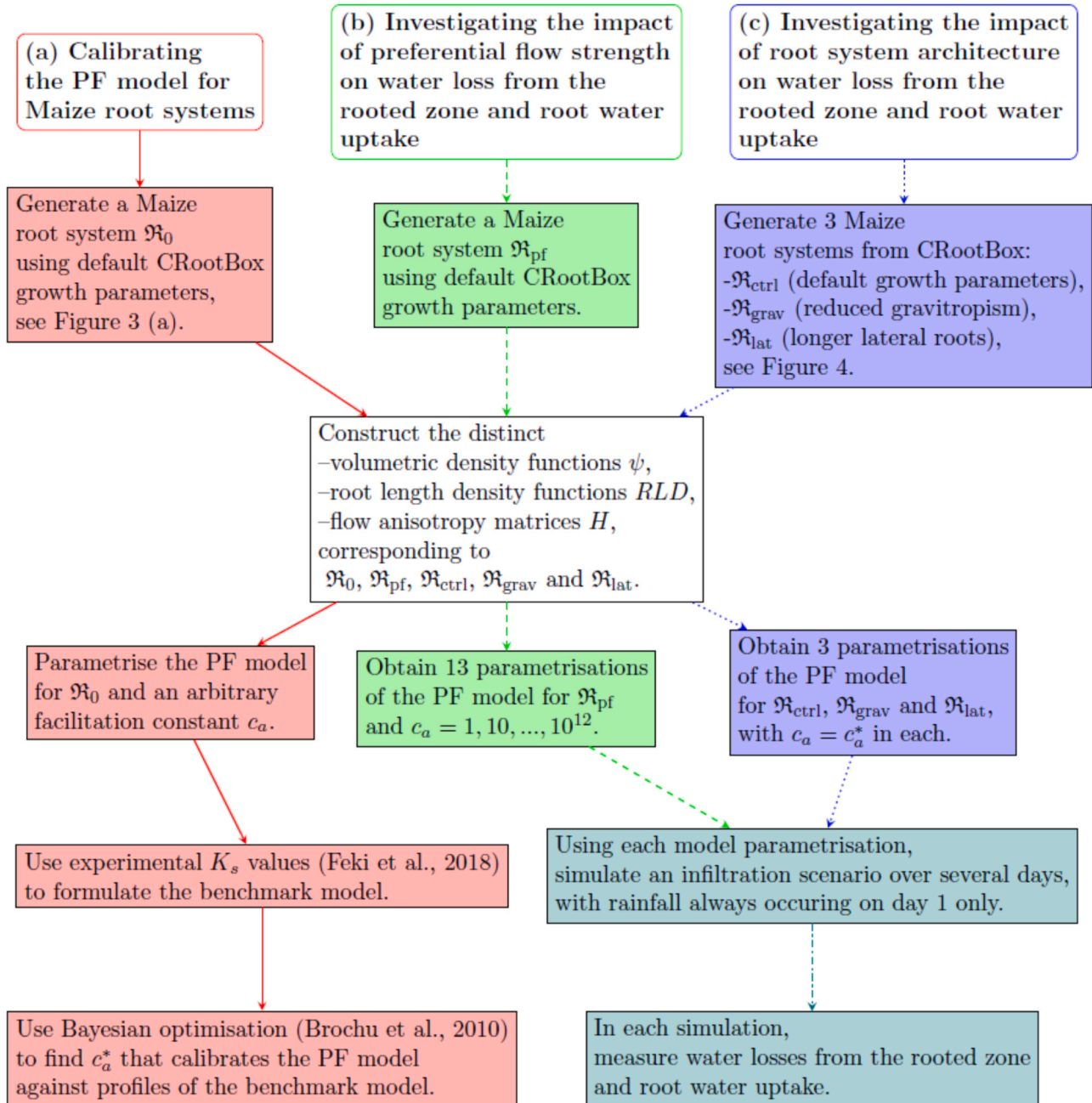


Fig. 2. Flowchart describing the methods employed to obtain the results of the work. (a) The solid red arrows and process boxes show the procedure for calibrating the PF model (Eqs. (1), (8)). (b) The dashed green arrows and green process boxes show the procedure for investigating the impact of preferential flow strength on water loss from the rooted zone and root water uptake. (c) The dotted blue arrows and blue process boxes show the procedure for investigating the impact or root architecture on water loss from the rooted zone and root water uptake. A white process box indicates a step that is common to all three procedures. A teal process box and a teal dot dash line indicates a process that is shared by procedures (b) and (c).

boundary, at the soil-atmosphere interface  $x_3 = 0$ , is denoted by  $\Gamma_1$  and is where water is lost via evaporation. Furthermore, the seeding location of the root system  $\mathfrak{R}$  is taken to be  $(0, 0, 0) \in \Gamma_1$ . The lower boundary and system rooting depth are denoted by  $\Gamma_3$  and  $D_{\mathfrak{R}}$  respectively. The lateral boundaries of the domain are denoted by  $\Gamma_2$  and water loss through these surfaces is assumed zero. The initial pressure head profile and boundary fluxes are then defined mathematically as

$$\begin{aligned} \tilde{\mathbf{q}} \cdot \mathbf{n} &= \tilde{q}_{\text{up}} & x \in \Gamma_1, t \in (0, T], \\ \tilde{\mathbf{q}} \cdot \mathbf{n} &= 0 & x \in \Gamma_2, t \in (0, T], \\ \tilde{\mathbf{q}} \cdot \mathbf{n} &= \tilde{q}_{\text{low}} & x \in \Gamma_3, t \in (0, T], \\ h(x, 0) &= h_0(x) & x \in \Omega. \end{aligned} \quad (8)$$

The water flux at the upper boundary is  $\tilde{q}_{\text{up}} = K_e ET_o - P_{\text{net}}$ . Here,  $P_{\text{net}} = P - RO$ , with  $P$  ( $LT^{-1}$ ) and  $RO$  ( $LT^{-1}$ ) being the precipitation and run off respectively. Evaporation is  $K_e ET_o$ , where  $K_e$  is a function of pressure head  $h$  that determines the proportion of total potential evapotranspiration coming from evaporation and the constant  $ET_o$  ( $LT^{-1}$ ) is the reference evapotranspiration (Allen et al., 1998). In the field, values for  $ET_o$  are calculated from meteorological data using the Penman-Monteith method. However, this work makes use of average  $ET_o$  values, for various agroclimatic regions, which are provided by Allen et al. (1998). We formulate a theoretical run off function as

$$RO(t, h) = \frac{P(t)}{\left(1 + \exp\left(-C\left(h + C^{-\frac{1}{2}}\right)\right)\right)}, \quad (9)$$

with  $C > 0$  being a large constant, so that if a section of soil on the upper surface is fully saturated ( $h = 0$ ), then  $RO(t, h) = P(t)$  and all

precipitation falling onto this section is lost as runoff instead of infiltrating into the soil. At the lower boundary  $\Gamma_3$ , a free drainage condition is imposed (Rassam et al., 2003):

$$\tilde{q}_{\text{low}} = [ -((1 - \psi) + H)(K_s \kappa(h) \mathbf{e}_3) ] \cdot \mathbf{n}, \quad (10)$$

where  $\mathbf{e}_3$  is the unit vector in the upward  $x_3$  direction. If not provided here, then explicit expressions for the functions discussed in this section are given in the supplementary material. Fig. 2 gives an overview of how the PF model (Eqs. (1), (8)) was calibrated against experimental data and subsequently employed to obtain the results of this work.

### 2.2. Parametrisation and calibration of the PF model

The majority of parameters in the PF model (Eqs. (1), (8)) were taken from existing literature. Values for  $K_s$  and the parameters in the hydraulic conductivity (Eq. (5)) and water retention functions (Eq. (4)) came from Carsel and Parrish (1988). The tortuosity in (Eq. (5)) was set to  $l = 0.5$  (Van Genuchten and Pachepsky, 2011), and parameter values in the functions for uptake and evaporation were taken from studies by Wesseling (1991), Allen et al. (1998) and Cai et al. (2018).

The *Zea mays 1* dataset of CRootBox was used to simulate 5 Maize root systems, each 90 days old, for which density functions and flow-anisotropy matrices were constructed in order to obtain corresponding parametrisations of the PF model (Eqs. (1), (8)). These root systems were assumed to be static during the time span of each simulated scenario. The first root system  $\mathfrak{R}_0$  was generated using the default growth parameters in the *Zea mays 1* dataset of CRootBox. These default values correspond to the parameter settings of an L-system model (Leitner

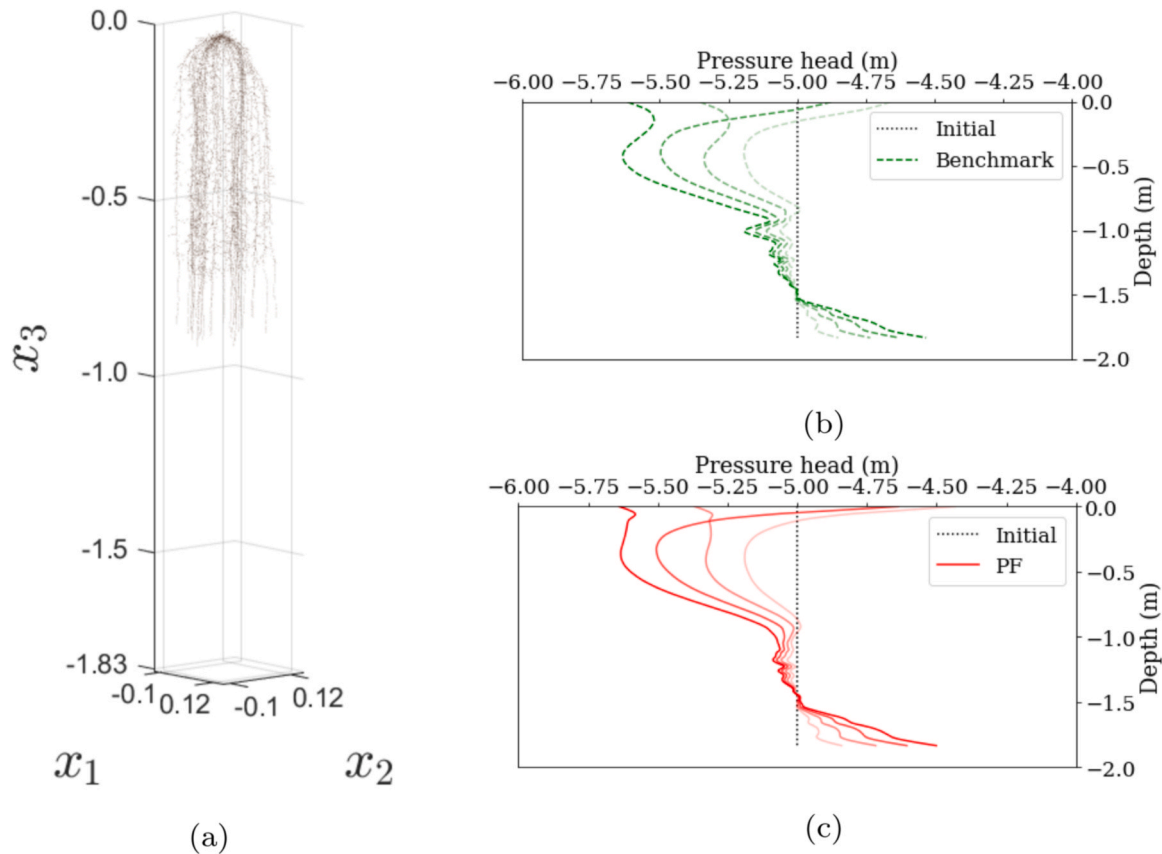


Fig. 3. The capacity of the PF model (Eqs. (1), (8)) to replicate pressure head profiles from the benchmark model. (a) Simulated Maize root system for which (i) benchmark pressure head profiles were obtained and (ii) the PF model (Eqs. (1), (8)) was parametrised. (b) The benchmark pressure head profiles generated for soil vegetated by the Maize root system shown in (a). (c) The pressure head profiles from the PF model (Eqs. (1), (8)), labelled “PF”, when calibrated with the facilitation constant  $c^*_a$  for the Maize root system in (a). In (b) and (c) lines of full opacity show pressure head profiles at the final time ( $T = 2$  days). Fainter lines show profiles at  $T = 0.5$ ,  $T = 1$  and  $T = 1.5$  days, with the opacity of the lines increasing with time.

et al., 2010b) that are required to generate virtual root architectures in agreement with the visual data of Kutschera (1960), which was obtained through excavation and precise illustration of Maize root systems. The root system  $\mathfrak{R}_0$  was then used to calibrate the PF model (Eqs. (1), (8)) against experimental data. Here, the soil domain was assumed to have lateral surfaces at the extremal points of  $\mathfrak{R}_0$  and reach twice as deep as rooting depth (Fig. 3(a)).

The second simulated root system  $\mathfrak{R}_{pf}$ , also obtained using default growth parameter values, was used to investigate the influence of preferential flow strength on uptake and water lifetime in the rooted zone. The final 3 simulated root systems were selected from known phenotypic variations and exhibited contrasting architectures. The total volume occupied by each was within a 2% tolerance of the others and these root systems were used to investigate the impact of root architectural traits on root water uptake and water lifetime in the rooted zone. One was a control root system,  $\mathfrak{R}_{ctrl}$ , generated using default growth parameter values (Fig. 4(a)). Another,  $\mathfrak{R}_{grav}$ , was generated with gravitropism parameters reduced so that its roots grew further in lateral directions before growing downward (Fig. 4(b)). The final root system  $\mathfrak{R}_{lat}$  was generated with growth parameter values that gave it similar characteristics to  $\mathfrak{R}_{ctrl}$ , but longer and fewer lateral roots and slightly shorter primary roots (Fig. 4(c)). The exact CRootBox parameter settings that were used to generate the five root systems described here can be found in Table 1 of the supplementary material.

Identical soil domains were used for each of the root systems  $\mathfrak{R}_{pf}$ ,  $\mathfrak{R}_{ctrl}$ ,  $\mathfrak{R}_{grav}$ , and  $\mathfrak{R}_{lat}$ . The four root systems all reached similar depths within the soil despite exhibiting contrasting architectures. Therefore, we were able to consider the same soil domain for each root system, which was defined as the smallest cuboid that could encompass any of the four root architectures. Deep percolation losses were then computed as the outward flux across the lower boundary of this domain. For simulations that considered a silt loam soil, an initial pressure head condition of  $h_0 = -5$  m was prescribed, which gave an initial water content  $\theta(h_0) = 0.214 \text{ m}^3 \text{ m}^{-3}$ . When considering other soil types, different values were set for  $h_0$  so that  $\theta(h_0) = 0.214 \text{ m}^3 \text{ m}^{-3}$  was maintained. Calibrating the PF model (Eqs. (1), (8)) involved using it to simulate the same infiltration scenario many times and therefore, to save computational time, the final time used in this scenario was limited to  $T = 2$  days. Investigating the impact of preferential flow strength on water lifetime required using the PF model to simulate an infiltration scenario at multiple different strengths of preferential flow and across a range of different soil types. Since the effects of increasing preferential flow strength on water lifetime in the rooted zone could be captured with a final time of  $T = 4$  days, the decision was taken to conserve computational time and not run these simulations past 4 days. In contrast, assessing the influence of root architectural traits on root water uptake and water loss from the rooted zone required far fewer simulations from the PF model (Eqs. (1), (8)). As a result, we allowed the final

time in this scenario to be extended to  $T = 7$  days. In the scenario used for calibration of the PF model, the precipitation condition  $P_0$  prescribed a single rainfall event on both days. For both the scenarios used to assess the influence of preferential flow strength and root architecture on root water lifetime in the rooted zone, we used a precipitation condition  $P$  that prescribed rainfall only on day 1. Expressions for  $P_0$  and  $P$  are detailed in the supplementary material. Tables 1, 2, and 3 in the supplementary material also provide specific sources for all parameters in the PF model (Eqs. (1), (8)) and show the values that were assigned.

The only parameter value left to determine in the PF model (Eqs. (1), (8)) was the axial facilitation constant  $c_a$ . This was achieved through calibration against experimental measurements of Feki et al. (2018), which identify a value  $K_s^* = 7.07 \text{ md}^{-1}$  for the saturated hydraulic conductivity of soil vegetated by a 90 day old Maize root system. Firstly, Richards equation was parametrised with a depth-dependent saturated hydraulic conductivity that took the value  $K_s^*$  in the vegetated section of soil and the value for fallow soil in the section below. By adding a sink term for the water uptake of root system  $\mathfrak{R}_0$  and equipping the equation with boundary and initial conditions equivalent to those in Eq. (8), a benchmark model was formed. Numerical pressure head profiles from this model provided a reference, for the effect of Maize root systems on soil hydraulic properties, against which the value of  $c_a$  in the PF model (Eqs. (1), (8)) could be calibrated.

A cost function  $u$  was then formulated whose minimiser  $c_a^*$  would estimate the facilitation constant value with which to parametrise the PF model (Eqs. (1), (8)) so that numerical pressure head profiles accurately matched the reference profiles provided by the benchmark model. Full details on the formulation of  $u$  and the benchmark model are given in the supplementary material. A Bayesian optimisation scheme (Brochu et al., 2010) was employed to find the minimiser  $c_a^*$  of the cost function. This method was chosen because it uses a probabilistic framework, which requires relatively few cost function evaluations to efficiently explore the parameter space, and does not rely on access to derivatives. These are desirable traits because evaluating  $u(c_a)$  for each different  $c_a$  involves the time intensive process of numerically solving the PF model (Eqs. (1), (8)).

### 2.3. Simulated scenarios

To investigate the influence of preferential flow strength on root water uptake and water lifetime in the rooted zone, the PF model (Eqs. (1), (8)) was parametrised for the root system  $\mathfrak{R}_{pf}$  and simulated for 13 different values of facilitation constant  $c_a$ . This started from  $c_a = 1$ , with the strength of preferential flow increasing as the value of  $c_a$  increased by factors of 10. These simulations were run for 7 soil types on the loam to clay spectrum (Carsel and Parrish, 1988).

For investigating the influence of root architecture on root water uptake and water lifetime in the rooted zone, the PF model (Eqs. (1), (8))

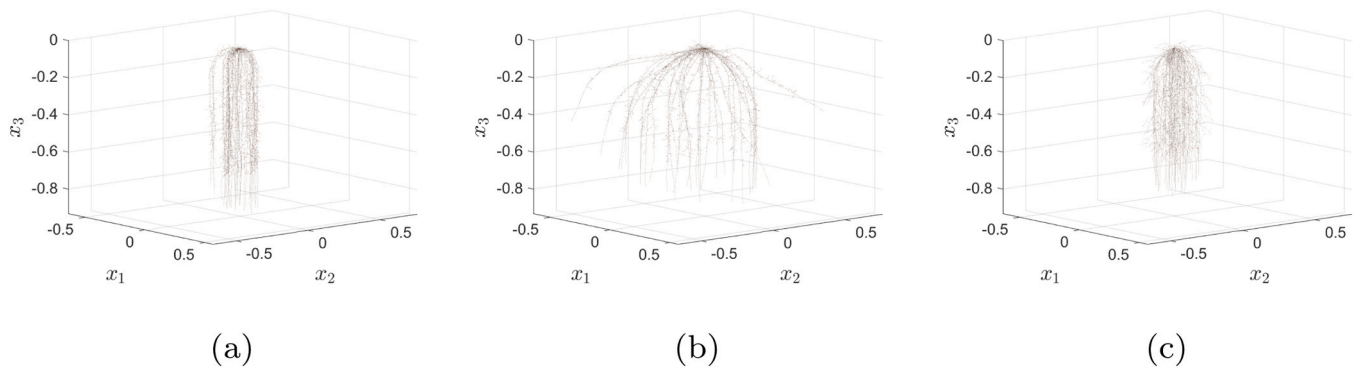


Fig. 4. Root systems used for testing the impact of root architectural traits on water loss from vegetated soil. (a) Control root system  $\mathfrak{R}_{ctrl}$ . (b) Root system where gravitropism of roots is decreased  $\mathfrak{R}_{grav}$ . (c) Root system where length of lateral roots is increased  $\mathfrak{R}_{lat}$ . The volumes that these root systems occupy are all within a 2% tolerance of each other.

was parametrised for each of the root systems  $\mathfrak{R}_{\text{ctrl}}$ ,  $\mathfrak{R}_{\text{grav}}$ , and  $\mathfrak{R}_{\text{lat}}$ . Simulations were obtained from each parametrisation, with the strength of induced preferential flow kept constant at  $c_a = c_a^*$  in all three. At the lower boundary  $\Gamma_3$ , the value of  $K_s$  was increased by a factor of 10 to impose a condition of enhanced free drainage. This modelled the situation of having a layer of more hydraulically conductive material at the lower boundary, which increases the rate of drainage and creates an effect similar to that of runoff along bedrock.

### 2.4. Computations

The conformal finite element method, with an implicit Euler discretisation in time, was used to obtain numerical pressure head solutions

to the PF model (Eqs. (1), (8)) and the benchmark model. The finite element mesh consisted of a disjoint union of tetrahedra, where the maximum possible circumradius of a tetrahedron was 0.059 m and the minimum was 0.029 m. A time step of 0.01d was used in the implicit Euler scheme and the linearisation of the water retention and hydraulic conductivity functions was achieved using an L-method (List and Radu, 2016). This finite element scheme was implemented using the FEniCS library (Alnæs et al. (2015)). The algorithms used to construct functions  $\psi$ ,  $H$ , and  $RLD$  were carried out in Python 3 using the NumPy and SciPy libraries (Harris et al., 2020). Root density profiles and simulations of water content evolution were visualised using Paraview (Ahrens et al., 2005). The plots in Figs. 3(a) and 4, showing the architectures of simulated root systems, were generated using MATLAB 2020a. The

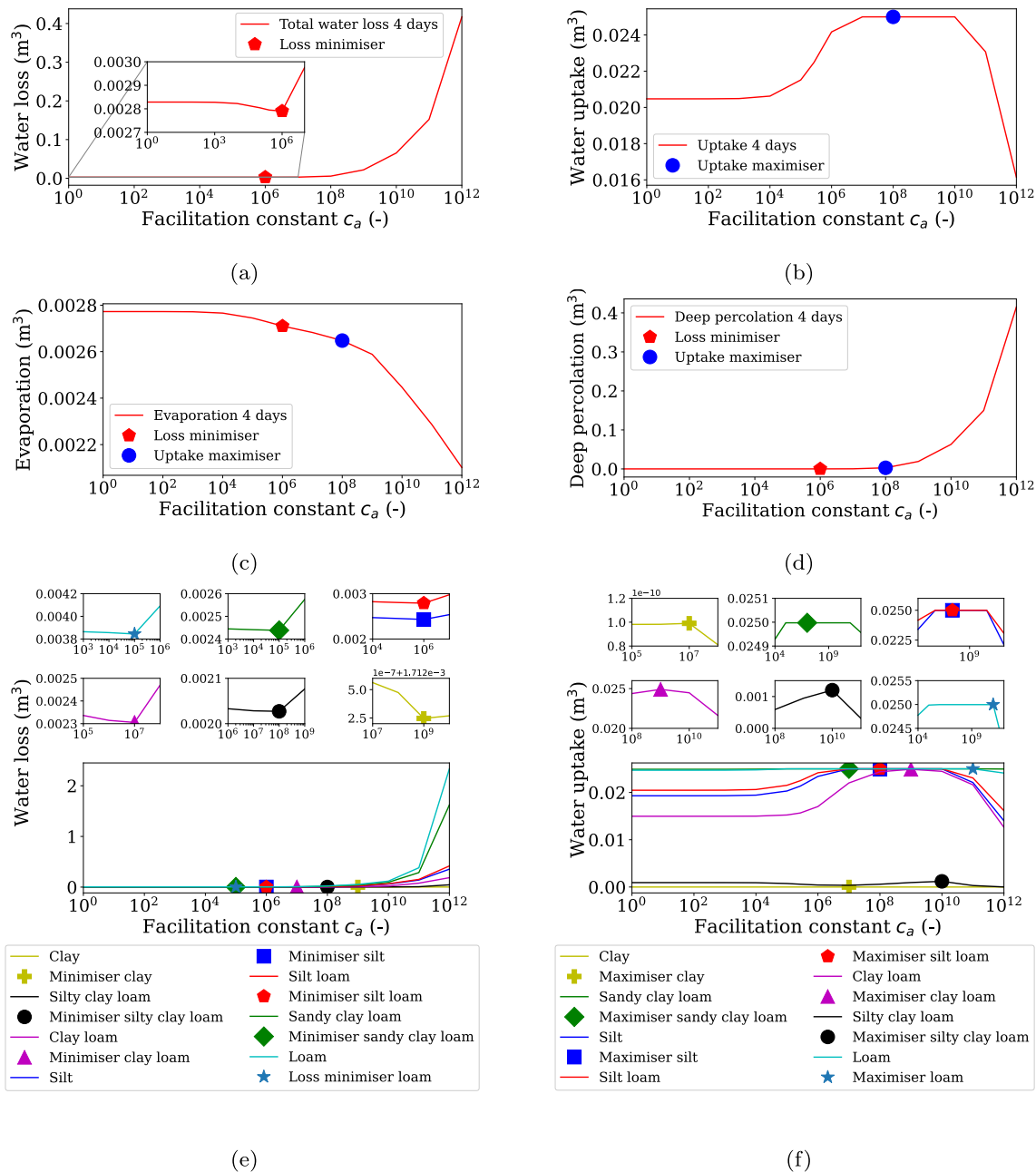


**Fig. 5.** The influence on water lifetime in the rooted zone from increasing and decreasing the strength of preferential flow induced by a root system. (a) Total water losses at increasing facilitation constant values  $c_a$  in silt loam soil. (b) Cumulative root water uptake at increasing  $c_a$  values in silt loam soil. (c) Water losses from evaporation at increasing  $c_a$  values in silt loam soil. (d) Water losses from deep percolation at increasing  $c_a$  values in silt loam soil. (e) Total water losses at increasing  $c_a$  values for all soil types. (f) Cumulative root water uptake at increasing  $c_a$  values for all soil types.

Bayesian optimisation algorithm used to find the optimal facilitation constant  $c_a^*$ , and hence calibrate the PF model, was implemented using the scikit-optimise library in Python 3 (Head et al., 2018).

### 3. Results

#### 3.1. Calibration of the PF model for Maize root systems

The PF model (Eqs. (1), (8)) was parametrised for the root system  $\mathfrak{N}_0$  (Fig. 3(a)) and  $H$  itself was parametrised with a facilitation constant  $c_a$ . For a given  $c_a$  value, the pressure head profile  $h_{c_a}$  was the numerical solution of the corresponding parametrisation of the PF model (Eqs. (1), (8)). A number of Bayesian optimisation schemes with low total iteration numbers were first run to search the interval [1,350000] for a  $c_a$  value that minimised the cost function  $u$ . Through this method, a trough in the value of  $u(c_a)$  was identified within the interval [268000,272000]. Since it is likely that the cost function  $u$  has a global minimiser (Mair et al., 2022), a further Bayesian optimisation scheme of 15 iterations was run on the interval [268000,272000]. This scheme identified a minimiser of  $c_a^* = 269782.377$ , where  $u(c_a^*) = 1.145$ . Since the final iterations of the scheme were clustered at points within a small neighbourhood of  $c_a^*$ , all yielding similarly low cost function values, the scheme was deemed to have sufficiently converged and no further iterations were performed. The close agreement between profiles  $h_{c_a^*}$ , from the PF model (Eqs. (1), (8)) calibrated with  $c_a^*$ , and profiles from the benchmark model is shown by Fig. 3(b) and (c). This indicates that our procedure is indeed capable of calibrating the PF model (Eqs. (1), (8)) against experimental data for Maize root systems.

#### 3.2. The impact of preferential flow strength on water loss from the rooted zone and root water uptake

All scenarios considered resulted in zero runoff losses. Total water loss from the rooted zone was therefore taken to be the sum of total evaporation and deep percolation. When considering the reference soil (silt loam), it was found that increasing the value of the facilitation constant from  $c_a = 1$  caused total cumulative evaporation losses to decrease (Fig. 5(c)). By contrast, total cumulative deep percolation losses were found to increase as the value of the facilitation constant was increased (Fig. 5(d)). This meant that total cumulative water loss decreased as the value of the facilitation constant increased from  $c_a = 1$  to a critical value of  $c_a \approx 10^6$  (Fig. 5(a)). However, for increases in  $c_a$  beyond this critical value, the increase in deep percolation losses exceeded the decrease in evaporation losses. This resulted in a net increase in water loss from the rooted zone (Fig. 5(a)). Similarly, cumulative root water uptake was found to increase as the facilitation constant was increased from  $c_a = 1$  but decrease once  $c_a$  was increased past some critical value (Fig. 5(b)). The same pattern was observed across all soil types considered but with different critical  $c_a$  values (Fig. 5 (e) and (f)).

Changing the strength of the preferential flow induced by the root system had the greatest impact on water loss in loam and sandy clay loam (Fig. 5(e)). Out of the soil types considered, these have the highest values for the saturated hydraulic conductivity  $K_s$  and water retention parameter  $\alpha_{vg}$  (Carsel and Parrish, 1988). On the other hand, for root water uptake, the strength of preferential flow had the largest effect in clay loam, silt and silt loam (Fig. 5(f)). These soil types have  $K_s$  and  $\alpha_{vg}$  values that are closest to the average over all seven types considered. For total water loss and root water uptake, the observed effect of changing the strength of root-induced preferential flow was smallest within clay and silty clay loam (Fig. 5(e), (f)). These soil types have the lowest values for  $K_s$  and  $\alpha_{vg}$  out of the seven considered.

#### 3.3. The impact of root system architecture on water loss from the rooted zone and root water uptake

Simulations from the PF model (Eqs. (1), (8)) showed zero runoff losses for the soils vegetated by the contrasting root systems shown in Fig. 4. Therefore, total water losses were a sum of evaporation and deep percolation. Results showed that cumulative total water loss from the rooted zone was greatest when the soil was vegetated by the control root system  $\mathfrak{N}_{ctrl}$ . They also showed that cumulative total water loss was lowest when the soil was vegetated by the root system  $\mathfrak{N}_{grav}$ , in which the gravitropism of roots had been reduced (Table 1). Over the entire simulation period, the rate of total water loss from the rooted zone ( $m^3 d^{-1}$ ) was lowest when it was vegetated by  $\mathfrak{N}_{grav}$  and highest when it was vegetated by  $\mathfrak{N}_{ctrl}$  (Fig. 6(a)).

For each of the soils vegetated by the 3 different root systems, approximately 15 – 20% of cumulative water loss was attributed to deep percolation. The losses via deep percolation were greatest within the soil vegetated by  $\mathfrak{N}_{ctrl}$ . The soils vegetated by  $\mathfrak{N}_{grav}$  and the system with longer lateral roots  $\mathfrak{N}_{lat}$  both exhibited lower values for cumulative deep percolation losses (Table 1). Deep percolation rate was highest, at all times of the simulation, within the soil vegetated by  $\mathfrak{N}_{ctrl}$ . This was particularly noticeable at early simulation times (Fig. 6(d)). To a lesser degree, the rate of deep percolation was higher when the soil was vegetated by  $\mathfrak{N}_{lat}$  as opposed to  $\mathfrak{N}_{grav}$ . Cumulative deep percolation losses were also marginally greater when the soil was vegetated by  $\mathfrak{N}_{lat}$  instead of  $\mathfrak{N}_{grav}$  (Table 1).

Regardless of root system, the majority of total soil water loss was always due to evaporation (Table 1). For the entire duration of the simulation, the rate of water loss via evaporation was lowest in the soil that was vegetated by  $\mathfrak{N}_{grav}$  (Fig. 6(a)). However, there was little difference, at any point in the simulation, between the rates of evaporation from the soils vegetated by  $\mathfrak{N}_{ctrl}$  and  $\mathfrak{N}_{lat}$  (Fig. 6(a)). In terms of cumulative evaporation, the soil vegetated by  $\mathfrak{N}_{grav}$  again lost the least. However, the soil vegetated by  $\mathfrak{N}_{lat}$  actually lost marginally more water via evaporation than the soil vegetated by  $\mathfrak{N}_{ctrl}$  (Table 1).

The water uptake performance of each root system followed an unsurprising trend. The cumulative root water uptake of  $\mathfrak{N}_{grav}$  was 29% higher than  $\mathfrak{N}_{ctrl}$  and 23% higher than  $\mathfrak{N}_{lat}$ . Furthermore,  $\mathfrak{N}_{lat}$  achieved a cumulative water uptake that was 4% higher than  $\mathfrak{N}_{ctrl}$  (Table 1). Further insight into these cumulative results is provided by the uptake rates of each root system over the seven day period (Fig. 6(b)). On the first two days, the root systems were all taking up water at the same maximum rate. On day 3, the water uptake rate of  $\mathfrak{N}_{ctrl}$  began to decline. This was followed by the uptake rate of  $\mathfrak{N}_{lat}$ , albeit with a shallower rate of decline. It was not until late in day 4 that the rate of uptake of  $\mathfrak{N}_{grav}$  started to decline, and the decline was considerably more shallow than for the other two root systems.

It was observed (Figs. 7 and 8) that each of the root systems in Fig. 4 induced different water flux patterns within the soil. Root-induced redistribution of soil water was driven by preferential flow and also

**Table 1**

Impact of root system architecture on water lifetime quantities. Results were computed using simulations of water transport from the PF model (Eqs. (1), (8)) when parametrised for root systems with different architectural characteristics (Fig. 4).

Root system	Cumulative water lifetime quantities ( $m^3$ )			
	Evaporation	Deep percolation	Total water loss	Water uptake
Control $\mathfrak{N}_{ctrl}$	$4.43 \times 10^{-3}$	$9.04 \times 10^{-4}$	$5.33 \times 10^{-3}$	$3.26 \times 10^{-2}$
Reduced gravitropism $\mathfrak{N}_{grav}$	$4.30 \times 10^{-3}$	$8.41 \times 10^{-4}$	$5.15 \times 10^{-3}$	$4.22 \times 10^{-2}$
Increased lateral length $\mathfrak{N}_{lat}$	$4.44 \times 10^{-3}$	$8.46 \times 10^{-4}$	$5.29 \times 10^{-3}$	$3.41 \times 10^{-2}$

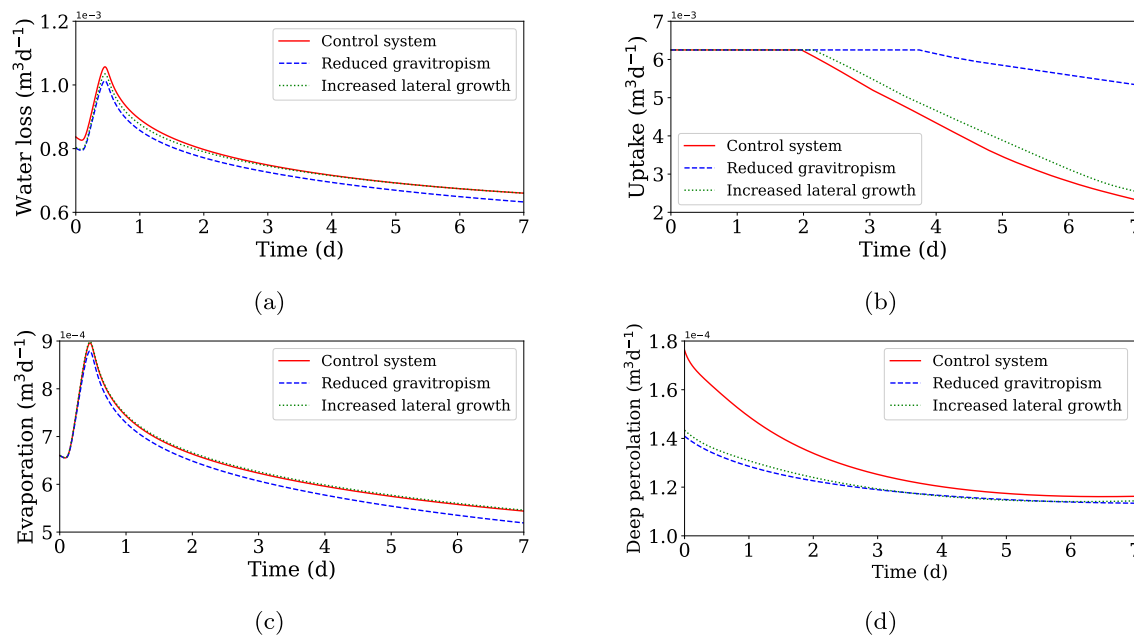


**Fig. 6.** Water losses and uptake rate from the rooted zone during a 7 day infiltration scenario, in 3 identically shaped soil domains, each vegetated by one of the root systems shown in Fig. 4, where there is precipitation on day 1 followed by 6 days of drought. (a) Rates of total water loss from the rooted zone. (b) Rates of total water uptake for each root system. (c) Rates of water loss from the rooted zone via evaporation. (d) Rates of water loss from the rooted zone via deep percolation.

the pressure gradients that arose from the removal of water by root uptake. At early stages of the simulation, the dominant effect of root system  $\mathfrak{N}_{\text{grav}}$  on soil water distribution was to facilitate increased infiltration from the soil surface into the bulk soil (Fig. 7(d)). This effect was observed across a larger area of the upper soil surface than in the soils vegetated by  $\mathfrak{N}_{\text{ctrl}}$  or  $\mathfrak{N}_{\text{lat}}$  (Figs. 8(a), (d) and (g)). For both  $\mathfrak{N}_{\text{ctrl}}$  and  $\mathfrak{N}_{\text{lat}}$ , the redistribution of soil water at early stages of the simulation was driven mainly by root water uptake from within the narrower regions of soil that they occupied (Figs. 7(a), (g)).

At all simulation times, the influence of  $\mathfrak{N}_{\text{grav}}$  on soil water transport spanned a greater lateral area than both  $\mathfrak{N}_{\text{ctrl}}$  and  $\mathfrak{N}_{\text{lat}}$  (Figs. 7, 8). This meant that, during later stages of the simulation,  $\mathfrak{N}_{\text{grav}}$  had facilitated the infiltration into bulk soil of a greater proportion of surface water than either of the other two root systems (Fig. 8). Consequently, in the period from the end of the precipitation event to the end of the simulation, the water content of the soil around  $\mathfrak{N}_{\text{grav}}$  was higher than in the soil around the other two root systems (Fig. 7).

## 4. Discussion

### 4.1. The trade-off between evaporation losses and losses by deep percolation

The environmental conditions experienced by many farmed crops lead to total water losses from the vegetated soil being dominated by evaporation, with a smaller proportion attributed to deep percolation (Paruelo and Sala, 1995; Schwinning and Sala, 2004). An increase in infiltration from the soil surface into the bulk soil will therefore reduce the amount of surface water vulnerable to evaporation without equivalently increasing deep percolation losses. This means that more water is available to the root system and for longer, which delays the emergence of water deficits and allows the plant to maintain a healthy rate of water uptake during periods of no precipitation.

In the PF model (Eqs. (1,8)), the strength of preferential flow induced by a root system can be increased by increasing the value of the facilitation constant  $c_a$ . Simulations showed that the  $c_a$  values that minimised total water loss and maximised root water uptake were orders of magnitude higher than the facilitation constant  $c_a^* = 269782.377$ ,

which was estimated from experimental data for Maize (Fig. 5). This indicates that Maize root systems may not increase infiltration into the bulk soil to an extent that is sufficient to minimise water loss. However, results also indicated that if the strength of root-induced preferential flow was increased too far, then the consequent increase in deep percolation losses would exceed the reduction in evaporation losses and cause a net increase in total water loss (Fig. 5). Similar results were obtained for all soil types considered. These showed that root systems in soils with higher hydraulic conductivity did not need to induce as strong a preferential flow to minimise water loss and maximise uptake (Fig. 5 (e),(f)).

Considering experimental research to date, there remains some doubt as to which root traits promote preferential flow through soil. However, potential candidates include root hair growth, the exudation of mucilage by root tissue, and the activity of the rhizosphere-microbiome, which have all been shown to affect the hydraulic characteristics of vegetated soil (Hallett et al., 2022; Carminati et al., 2010; Choudhury et al., 2018). Through breeding, it is possible to produce phenotypes that vary in their expression of these traits (Hochholdinger and Tuberosa, 2009; Ahmad et al., 2011; Bilyera et al., 2021). This suggests that selecting specific phenotypes, which induce preferential flow to an extent that is optimal for extending the lifetime of water in the soil type they inhabit, may provide a new strategy for developing drought resistant crops.

### 4.2. The effect of root system architecture on water lifetime in vegetated soil

Following precipitation, root-oriented preferential flow influences patterns of infiltration into soil (Noguchi et al., 1997). Because of this, root systems with differing architectures are likely to induce different distributions of water throughout the soil. The presence of roots near the surface of soil has been observed in experiments to increase infiltration rates into bulk soil (Song et al., 2017; Leung et al., 2018). This increased infiltration can be attributed initially to roots near the soil surface inducing preferential downward flow, then subsequently to roots removing water from the soil via uptake and steepening the pressure head gradient between upper and lower soil layers. The mass of the

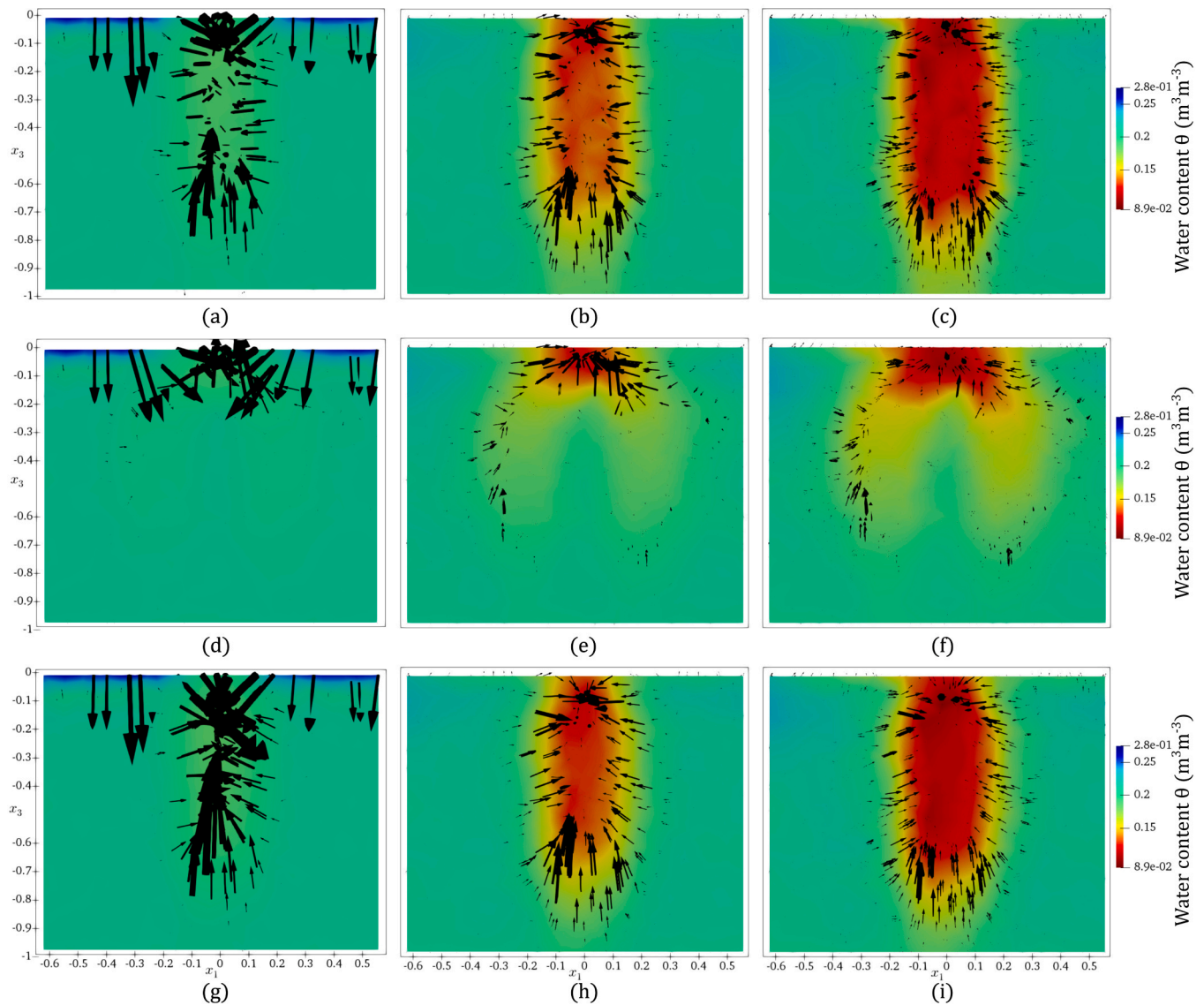


**Fig. 7.** Evolution of post precipitation soil water content in the rooted zone. Three identical silt loam domains, each vegetated with one of the root systems in Fig. 4. The plot shows cross sections taken at  $x_2 = 0.05$ , the midpoint of the domain in the  $x_2$  direction, where the  $x$  axis gives the lateral  $x_1$  location and the  $y$  axis gives the depth in the soil  $x_3$ . Plots (a), (d), (g) show water content profiles after 0.5 days for soils vegetated by the control  $\mathfrak{R}_{\text{ctrl}}$ , the reduced gravitropism  $\mathfrak{R}_{\text{grav}}$ , and the increased lateral growth  $\mathfrak{R}_{\text{lat}}$  root systems respectively. Following the same order, plots (b), (e), (h) show water content profiles after 3.75 days, and plots (c), (f), (i) show profiles after 7 days. Arrows indicate the direction and strength of the water flux in different regions of the domain, which is being influenced both by the steepening of pressure head gradients as a result of root water uptake and the preferential flow induced by the root system. These factors influence each other in a nonlinear way and, hence, cannot be decoupled into arrows that correspond to each process.

reduced gravitropism root system  $\mathfrak{R}_{\text{grav}}$  is distributed over a larger lateral area than the other systems (Fig. 4). This was particularly true at shallower soil depths. Therefore, by the mechanisms mentioned above,  $\mathfrak{R}_{\text{grav}}$  increased infiltration from surface soil to bulk across a larger lateral area of the domain (Fig. 8). For this reason, in comparison to the other root systems, less soil water was left at the surface and, hence, less water was lost to evaporation.

Water losses via deep percolation were lowest in the soil vegetated by  $\mathfrak{R}_{\text{grav}}$  and highest, by a considerable margin, in the soil vegetated by the control root system  $\mathfrak{R}_{\text{ctrl}}$  (Table 1). Reduced gravitropism and longer first-order laterals mean a smaller proportion of total root length is oriented vertically downward than in a system with typical root architecture like  $\mathfrak{R}_{\text{ctrl}}$  (Fig. 4). Consequently, these root systems divert more soil water transport into lateral directions than  $\mathfrak{R}_{\text{ctrl}}$ , which means less water will pass the lower boundary of the rooted zone. Secondly, if roots take up water, then that water is not lost via deep percolation. Moreover,

the removal of water via uptake will steepen pressure head gradients within the soil and drive more capillary rise. Compared to  $\mathfrak{R}_{\text{grav}}$ , root water uptake by  $\mathfrak{R}_{\text{ctrl}}$  and  $\mathfrak{R}_{\text{lat}}$  was concentrated within a narrower region of the soil (Figs. 7 and 8). As a result, capillary rise was induced within a narrower region of the soil (Fig. 7) and more water was lost from the soil via deep percolation.

Since the soil with the root system  $\mathfrak{R}_{\text{grav}}$  lost the least water to evaporation and deep percolation (Fig. 6, Table 1), it is unsurprising that this root system maintained the highest uptake rate at all simulation times. We do however propose one more contributing factor toward this result. Because the root mass of  $\mathfrak{R}_{\text{grav}}$  is distributed over the greatest volume of soil (Fig. 4), uptake is not limited to narrow soil regions in the way it is for  $\mathfrak{R}_{\text{ctrl}}$  and  $\mathfrak{R}_{\text{lat}}$  (Figs. 7, 8). This means that the water available to  $\mathfrak{R}_{\text{grav}}$  is depleted less quickly, thus allowing it to maintain its uptake rate over longer periods (Fig. 6(d)). All these findings lead us to the conclusion that, in scenarios involving intermittent precipitation events

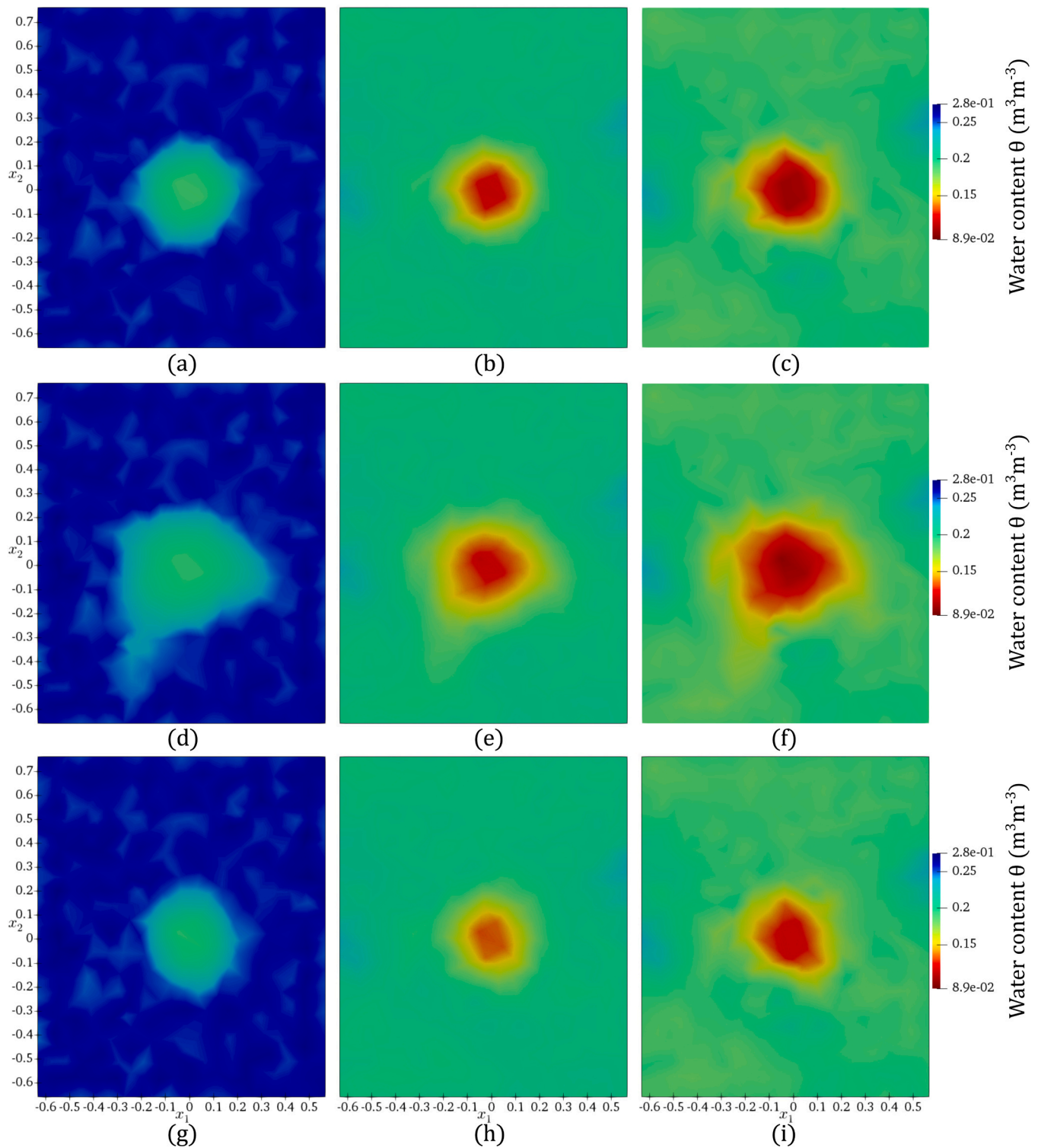


**Fig. 8.** Evolution of post precipitation soil water content in the rooted zone of three identical silt loam domains, each vegetated with one of the root systems in Fig. 4. The view looks down on the upper soil surface ( $x_3 = 0$ ), with the  $x$  and  $y$  axes giving the position in the lateral  $x_1$  and  $x_2$  dimensions respectively. Plots (a), (d), (g) show water content profiles after 0.5 days for soils vegetated by the control  $\mathfrak{R}_{ctrl}$ , the reduced gravitropism  $\mathfrak{R}_{grav}$ , and the increased lateral growth  $\mathfrak{R}_{lat}$  root systems respectively. Following the same order, plots (b), (e), (h) show water content profiles after 3.75 days and plots (c), (f), (i) show profiles after 7 days.

followed by periods of drought, Maize root systems with reduced gravitropism (Fig. 4(b)) are most adept at extending water lifetime in the rooted zone and maximising uptake efficiency.

#### 4.3. Root system ideotypes for drought resistance

Numerous morphological and physiological features of plant roots are involved in the acquisition of water and nutrients from soil. The length and density of root hairs is critical to the uptake of immobile nutrients such as phosphorous and potassium (Jungk, 2001). For

accessing mobile resources such as nitrogen and water, structural traits like root growth angle have been shown to play a crucial role (Uga et al., 2013). In terms of physiological adaptations, experimental investigations have revealed that some plants form root cortical aerenchyma as a response to the effects of drought conditions (Zhu et al., 2010) and soil water logging (Yamauchi et al., 2018). Furthermore, the exudation of mucilage by plant roots is known to influence the composition and activity of the root microbiome (Badri and Vivanco, 2009). This affects the hydraulic characteristics of the rhizosphere (de la Fuente Cantó et al., 2020) and the radial hydraulic conductivity of the root tissue, which in turn influences the capacity of the root to absorb water and nutrients (Pierret, 2022).

There is some disagreement as to exactly what a root ideotype for water use efficiency and drought resistance should look like (Tardieu, 2012; Tron et al., 2015; Pierret, 2022). The influential study of Lynch (2013) concluded that drought resistant root systems must be “steep, cheap and deep” (SCD) i.e. have large diameter primary roots that grow deep with fewer, but longer, laterals (Nepstad et al., 1994; Schenk and Jackson, 2002; Lynch and Wojciechowski, 2015). This was later supported by the experimental results of Uga et al. (2013). The justification for SCD root systems comes from the premise that such an architecture allows access to water stored at greater depths, with the presence of some root mass near the soil surface meaning uptake at shallower depths is not overly compromised (Lynch, 2013). However, when considering an initial condition of higher water content near the soil surface, the simulations of Leitner et al. (2014) found that an SCD maize root system achieved a lower cumulative water uptake than one with a standard structure. Lynch (2013) also concedes that in semi-arid climates, where intermittent periods of drought are punctuated by regular rainfall events, the advantage of an SCD root system structure is less obvious. Simulation-based and experimental results have provided supporting evidence of this in the context of wheat and barley (Manschadi et al., 2006) as well as for a number of desert shrubs (Xu et al., 2017) and cacti (Snyman, 2006). Furthermore, recent work by Clément et al. (Clément et al., 2022) has shown that the axial hydraulic conductivity of root tissue decreases with depth, which suggests that SCD root systems may be unable to effectively utilize all the deeply stored water that their architectures provide them access to.

Since soil water content is very dynamic, we propose a departure from the approach to identifying root system ideotypes for drought resistance that focuses solely on the spatial distribution of roots and the capacity to access static stores of soil water. Instead, we emphasise the capacity of root systems to induce preferential flow patterns, as a result of their architecture and physiological activity, which increase the lifetime of water in the rooted soil by decreasing losses via evaporation and deep percolation. This incorporates traits that influence the characteristics of the surrounding soil into the concept of a root system ideotype for drought resistance. Such a perspective is an example of the concept of an extended phenotype for drought resistance (de la Fuente Cantó et al., 2020). For plants that feed on water accumulated at great depths, this perspective is still likely to identify the SCD root system as optimal (Lynch, 2013). However, if crops are rain fed (or irrigated by sprinklers) and experience periods of intermittent drought, then root systems with reduced gravitropism may indeed make the most efficient use of water. Further experimental research is required to validate the conclusions of this work and provide more evidence that root-oriented preferential flow is a crucial factor to consider when identifying crop ideotypes for drought resistance.

#### Declaration of Competing Interest

The authors declare that they have no known competing financial interests or personal relationships that could have appeared to influence the work reported in this paper.

#### Data Availability

Data will be made available on request.

#### Acknowledgements

Andrew Mair was supported by The Maxwell Institute Graduate School in Analysis and its Applications, a Centre for Doctoral Training funded by the UK Engineering and Physical Sciences Research Council (grant EP/L016508/01), the Scottish Funding Council, Heriot-Watt University and the University of Edinburgh. Lionel Dupuy was supported by the Spanish Ministry of Science and Innovation (MICINN) under the project MICROCROWD (PID2020-112950RR-I00).

#### Appendix A. Supporting information

Supplementary data associated with this article can be found in the online version at doi:10.1016/j.fcr.2023.109006.

#### References

- Ahmad, S., Veyrat, N., Gordon-Weeks, R., Zhang, Y., Martin, J., Smart, L., Glauser, G., Erb, M., Flors, V., Frey, M., et al., 2011. Benzoxazinoid metabolites regulate innate immunity against aphids and fungi in maize. *Plant Physiol.* 157, 317–327.
- Ahmed, M.A., Kroener, E., Benard, P., Zarebanadkouki, M., Kaestner, A., Carminati, A., 2016. Drying of mucilage causes water repellency in the rhizosphere of maize: measurements and modelling. *Plant Soil* 407, 161–171.
- Ahrens, J., Geveci, B., Law, C., 2005. Paraview: An end-user tool for large data visualization. *Vis. Handb.* 717.
- Allen, R.G., Pereira, L.S., Raes, D., Smith, M., et al., 1998. Crop evapotranspiration—guidelines for computing crop water requirements—Fao irrigation and drainage paper 56. Fao, Rome 300, D05109.
- Alnæs, M.S., Blechta, J., Hake, J., Johansson, A., Kehlet, B., Logg, A., Richardson, C., Ring, J., Rognes, M.E., Wells, G.N., et al., 2015. The fenics project version 1.5. *Arch. Numer. Softw.* 3. <https://doi.org/10.11588/ans.2015.100.20553>.
- Anselmucci, F., Andò, E., Viggiani, G., Lenoir, N., Arson, C., Sibille, L., 2021. Imaging local soil kinematics during the first days of maize root growth in sand. *Sci. Rep.* 11, 1–13.
- Badri, D.V., Vivanco, J.M., 2009. Regulation and function of root exudates. *Plant, Cell Environ.* 32, 666–681.
- Beff, L., Günther, T., Vandoorne, B., Couvreur, V., Javaux, M., 2013. Three-dimensional monitoring of soil water content in a maize field using electrical resistivity tomography. *Hydrol. Earth Syst. Sci.* 17, 595–609.
- Bethune, M., Selle, B., Wang, Q., 2008. Understanding and predicting deep percolation under surface irrigation. *Water Resour. Res.* 44.
- Bilyera, N., Zhang, X., Duddek, P., Fan, L., Banfield, C.C., Schlüter, S., Carminati, A., Kaestner, A., Ahmed, M.A., Kuzakov, Y., et al., 2021. Maize genotype-specific exudation strategies: an adaptive mechanism to increase microbial activity in the rhizosphere. *Soil Biol. Biochem.* 162, 108426.
- Brochu, E., Cora, V.M., De Freitas, N., 2010. A tutorial on bayesian optimization of expensive cost functions, with application to active user modeling and hierarchical reinforcement learning. *arXiv preprint arXiv:1012.2599*.
- Bruand, A., Cousin, I., Nicoullaud, B., Duval, O., Begon, J.C., 1996. Backscattered electron scanning images of soil porosity for analyzing soil compaction around roots. *Soil Sci. Soc. Am. J.* 60, 895–901.
- Buckingham, E., 1907. Studies on the movement of soil moisture.
- Cai, G., Vanderborght, J., Couvreur, V., Mboh, C.M., Vereecken, H., 2018. Parameterization of root water uptake models considering dynamic root distributions and water uptake compensation. *Vadose Zone J.* 17, 1–21.
- Cal, A.J., Sanciangco, M., Rebollo, M.C., Luquet, D., Torres, R.O., McNally, K.L., Henry, A., 2019. Leaf morphology, rather than plant water status, underlies genetic variation of rice leaf rolling under drought. *Plant, Cell Environ.* 42, 1532–1544.
- Carminati, A., Moradi, A.B., Vetterlein, D., Vontobel, P., Lehmann, E., Weller, U., Vogel, H.J., Oswald, S.E., 2010. Dynamics of soil water content in the rhizosphere. *Plant Soil* 332, 163–176.
- Carsel, R.F., Parrish, R.S., 1988. Developing joint probability distributions of soil water retention characteristics. *Water Resour. Res.* 24, 755–769.
- Choudhury, B., Ferraris, S., Ashton, R., Powelson, D., Whalley, W., 2018. The effect of microbial activity on soil water diffusivity. *Eur. J. Soil Sci.* 69, 407–413.
- Clausnitzer, V., Hopmans, J., 1994. Simultaneous modeling of transient three-dimensional root growth and soil water flow. *Plant Soil* 164, 299–314.
- Clément, C., Schneider, H.M., Dresbøll, D.B., Lynch, J.P., Thorup-Kristensen, K., 2022. Root and xylem anatomy varies with root length, root order, soil depth and environment in intermediate wheatgrass (kernza®) and alfalfa. *Annals of Botany*.
- Danjon, F., Bert, D., Godin, C., Trichet, P., 1999. Structural root architecture of 5-year-old Pinus pinaster measured by 3d digitising and analysed with amapmod. *Plant Soil* 217, 49–63.
- Darcy, H.P. G., 1856. Les Fontaines publiques de la ville de Dijon. Exposition et application des principes à suivre et des formules à employer dans les questions de distribution d'eau, etc. V. Dalmont.

- Dexter, A., 1987. Compression of soil around roots. *Plant Soil* 97, 401–406.
- Doussan, C., Vercambre, G., PAGÈ, L., 1998. Modelling of the hydraulic architecture of root systems: an integrated approach to water absorption—distribution of axial and radial conductances in maize. *Ann. Bot.* 81, 225–232.
- Doussan, C., Pierret, A., Garrigues, E., Pagès, L., 2006. Water uptake by plant roots: li-by plant roots: li - modelling of water transport in the soil root-system with explicit account of flow within the root system – comparison with experiments. *Plant Soil* 283, 99–117.
- Draye, X., Kim, Y., Lobet, G., Javaux, M., 2010. Model-assisted integration of physiological and environmental constraints affecting the dynamic and spatial patterns of root water uptake from soils. *J. Exp. Bot.* 61, 2145–2155.
- Fang, Y., Xiong, L., 2015. General mechanisms of drought response and their application in drought resistance improvement in plants. *Cell. Mol. Life Sci.* 72, 673–689.
- Feddes, R.A., 1982. Simulation of field water use and crop yield. In: *Simulation of plant growth and crop production*. Pudoc, pp. 194–209.
- Feehey, D.S., Crawford, J.W., Daniell, T., Hallett, P.D., Nunan, N., Ritz, K., Rivers, M., Young, I.M., 2006. Three-dimensional microorganization of the soil–root–microbe system. *Microb. Ecol.* 52, 151–158.
- Feki, M., Ravazzani, G., Ceppi, A., Mancini, M., 2018. Influence of soil hydraulic variability on soil moisture simulations and irrigation scheduling in a maize field. *Agric. Water Manag.* 202, 183–194.
- Frensch, J., Steudle, E., 1989. Axial and radial hydraulic resistance to roots of maize (*Zea mays* L.). *Plant Physiol.* 91, 719–726.
- de la Fuente Cantó, C., Simonin, M., King, E., Moulin, L., Bennett, M.J., Castrillo, G., Laplace, L., 2020. An extended root phenotype: the rhizosphere, its formation and impacts on plant fitness. *Plant J.* 103, 951–964.
- Gerke, H.H., Van Genuchten, M.T., 1993. A dual-porosity model for simulating the preferential movement of water and solutes in structured porous media. *Water Resour. Res.* 29, 305–319.
- Ghestem, M., Sidle, R.C., Stokes, A., 2011. The influence of plant root systems on subsurface flow: implications for slope stability. *Bioscience* 61, 869–879.
- Goodwin, S.M., Jenks, M.A., 2005. Plant cuticle function as a barrier to water loss. *Plant Abiotic Stress* 14–36.
- Hallett, P., Marin, M., Feehey, D.S., Brown, L., Naveed, M., Koebnick, N., Ruiz, C., Bengough, A.G., Roose, T., George, T., 2022. Impact of root hairs on microscale soil physical properties in the field. *Plant Soil*.
- Harris, C.R., Millman, K.J., van der Walt, S.J., Gommers, R., Virtanen, P., Cournapeau, D., Wieser, E., Taylor, J., Berg, S., Smith, N.J., et al., 2020. Array programming with numpy. *Nature* 585, 357–362.
- Head, T., MechCoder, Louppe, G., Shcherbatyi, I., fcharras, Vinicius, Z., cmmalone, Schröder, C., nel215, Campos, N., Young, T., Cereda, S., Fan, T., rene rex, Shi, K.K., Schwabedal, J., carlosdanielcsantos, Hvass-Labs, Pak, M., SoManyUsernamesTaken, Callaway, F., Estève, L., Besson, L., Cherti, M., Pfannschmidt, K., Linzberger, F., Caet, C., Gut, A., Mueller, A., Fabisch, A., 2018. scikit-optimize/scikit-optimize: v0.5.2.10.5281/zenodo.1207017.
- Hochhöltinger, F., Tuberosa, R., 2009. Genetic and genomic dissection of maize root development and architecture. *Curr. Opin. Plant Biol.* 12, 172–177.
- Hose, E., Clarkson, D.T., Steudle, E., Schreiber, U., Hartung, W., 2001. The exodermis: a variable apoplastic barrier. *J. Exp. Bot.* 52, 2245–2264.
- Javaux, M., Schroder, T., Vanderborght, J., Vereecken, H., 2008. Use of a three-dimensional detailed modeling approach for predicting root water uptake. *Vadose Zone J.* 7, 1079–1088.
- Jungk, A., 2001. Root hairs and the acquisition of plant nutrients from soil. *J. Plant Nutr. Soil Sci.* 164, 121–129.
- Keating, B.A., Carberry, P.S., Hammer, G.L., Probert, M.E., Robertson, M.J., Holzworth, D., Huth, N.I., Hargreaves, J.N., Meinke, H., Hochman, Z., et al., 2003. An overview of apsim, a model designed for farming systems simulation. *Eur. J. Agron.* 18, 267–288.
- Koch, A., Meunier, F., Vanderborght, J., Garré, S., Pohlmeier, A., Javaux, M., 2019. Functional-structural root-system model validation using a soil MRI experiment. *J. Exp. Bot.* 70, 2797–2809.
- Koebnick, N., Daly, K.R., Keyes, S.D., Bengough, A.G., Brown, L.K., Cooper, L.J., George, T.S., Hallett, P.D., Naveed, M., Raffan, A., et al., 2019. Imaging microstructure of the barley rhizosphere: particle packing and root hair influences. *N. Phytol.* 221, 1878–1889.
- Kutschera, L., et al., 1960. Root atlas of central European crop plants and weeds of arable land. *Root Atlas Cent. Eur. Crop Plants Weeds Arable Land*.
- Lange, B., Lüescher, P., Germann, P.F., 2009. Significance of tree roots for preferential infiltration in stagnic soils. *Hydrol. Earth Syst. Sci.* 13, 1809–1821.
- Leitner, D., Klepsch, S., Bodner, G., Schnepf, A., 2010a. A dynamic root system growth model based on I-systems: tropisms and coupling to nutrient uptake from soil. *Plant Soil* 332, 177–192.
- Leitner, D., Klepsch, S., Knieß, A., Schnepf, A., 2010b. The algorithmic beauty of plant roots—an I-system model for dynamic root growth simulation. *Math. Comput. Model. Dyn. Syst.* 16, 575–587.
- Leitner, D., Meunier, F., Bodner, G., Javaux, M., Schnepf, A., 2014. Impact of contrasted maize root traits at flowering on water stress tolerance—a simulation study. *Field Crops Res.* 165, 125–137.
- Leung, A., Boldrin, D., Liang, T., Wu, Z., Kamchoom, V., Bengough, A., 2018. Plant age effects on soil infiltration rate during early plant establishment. *Géotechnique* 68, 646–652.
- Li, B., Wei, A., Song, C., Li, N., Zhang, J., 2008. Heterologous expression of the *tsvp* gene improves the drought resistance of maize. *Plant Biotechnol. J.* 6, 146–159.
- List, F., Radu, F.A., 2016. A study on iterative methods for solving richards' equation. *Comput. Geosci.* 20, 341–353.
- Liu, B., Zeng, F.J., Arndt, S.K., He, J.X., Luo, W.C., Song, C., 2013. Patterns of root architecture adaptation of a phreatophytic perennial desert plant in a hyperarid desert. *South Afr. J. Bot.* 86, 56–62.
- Lopes, M.S., Reynolds, M.P., 2010. Partitioning of assimilates to deeper roots is associated with cooler canopies and increased yield under drought in wheat. *Funct. Plant Biol.* 37, 147–156.
- Lowe, M.A., McGrath, G., Mathes, F., Leopold, M., 2017. Evaluation of surfactant effectiveness on water repellent soils using electrical resistivity tomography. *Agric. Water Manag.* 181, 56–65.
- Luo, L., 2010. Breeding for water-saving and drought-resistance rice (wdr) in china. *J. Exp. Bot.* 61, 3509–3517.
- Lynch, J.P., 2013. Steep, cheap and deep: an ideotype to optimize water and n acquisition by maize root systems. *Ann. Bot.* 112, 347–357.
- Lynch, J.P., Wojciechowski, T., 2015. Opportunities and challenges in the subsoil: pathways to deeper rooted crops. *J. Exp. Bot.* 66, 2199–2210.
- Mair, A., Dupuy, L.X., Ptashnyk, M., 2022. Model for water infiltration in vegetated soil with preferential flow oriented by plant roots. *Plant Soil* 1–21.
- Manschadi, A.M., Christopher, J., deVoil, P., Hammer, G.L., 2006. The role of root architectural traits in adaptation of wheat to water-limited environments. *Funct. Plant Biol.* 33, 823–837.
- Michot, D., Benderitter, Y., Dorigny, A., Nicoullaud, B., King, D., Tabbagh, A., 2003. Spatial and temporal monitoring of soil water content with an irrigated corn crop cover using surface electrical resistivity tomography. *Water Resour. Res.* 39.
- Mualem, Y., 1976. A new model for predicting the hydraulic conductivity of unsaturated porous media. *Water Resour. Res.* 12, 513–522.
- Naveed, M., Brown, L.K., Raffan, A., George, T.S., Bengough, A., Roose, T., Sinclair, I., Koebnick, N., Cooper, L., Hallett, P.D., 2018. Rhizosphere-scale quantification of hydraulic and mechanical properties of soil impacted by root and seed exudates. *Vadose Zone J.* 17.
- Naveed, M., Ahmed, M.A., Benard, P., Brown, L.K., George, T., Bengough, A., Roose, T., Koebnick, N., Hallett, P., 2019. Surface tension, rheology and hydrophobicity of rhizodeposits and seed mucilage influence soil water retention and hysteresis. *Plant Soil* 437, 65–81.
- Nepstad, D.C., de Carvalho, C.R., Davidson, E.A., Jipp, P.H., Lefebvre, P.A., Negreiros, G. H., daSilva, E.D., Stone, T.A., Trumbore, S.E., Vieira, S., 1994. The role of deep roots in the hydrological and carbon cycles of amazonian forests and pastures. *Nature* 372, 666–669.
- Noguchi, S., Nik, A.R., Kasran, B., Tani, M., Sammori, T., Morisada, K., 1997. Soil physical properties and preferential flow pathways in tropical rain forest, bukit terek, peninsular malaysia. *J. For. Res.* 2, 115–120.
- Pages, L., Jordan, M.O., Picard, D., 1989. A simulation model of the three-dimensional architecture of the maize root system. *Plant Soil* 119, 147–154.
- Pages, L., Vercambre, G., Drouet, J.L., Lecomte, F., Collet, C., LeBot, J., 2004. Root typ: a generic model to depict and analyse the root system architecture. *Plant Soil* 258, 103–119.
- Paruelo, J.M., Sala, O.E., 1995. Water losses in the patagonian steppe: a modelling approach: ecological archives e076-001. *Ecology* 76, 510–520.
- Pierret, A., 2022. Will deeper roots be enough? engineering drought-resistant crops will entail in-depth understanding of root hydraulic architecture. a commentary on 'root and xylem anatomy varies with root length, root order, soil depth and environment. *Ann. Bot.*
- Postma, J.A., Kuppe, C., Owen, M.R., Mellor, N., Griffiths, M., Bennett, M.J., Lynch, J.P., Watt, M., 2017. Opensimroot: widening the scope and application of root architectural models. *N. Phytol.* 215, 1274–1286.
- Rassam, D., Simunek, J., Van Genuchten, M.T., 2003. Modelling variably saturated flow with HYDRUS-2D. ND Consult Brisbane, Australia.
- Read, D., Bengough, A.G., Gregory, P.J., Crawford, J.W., Robinson, D., Scrimgeour, C., Young, I.M., Zhang, K., Zhang, X., 2003. Plant roots release phospholipid surfactants that modify the physical and chemical properties of soil. *N. Phytol.* 157, 315–326.
- Richards, L.A., 1931. Capillary conduction of liquids through porous mediums. *Physics* 1, 318–333.
- Schenk, H.J., Jackson, R.B., 2002. Rooting depths, lateral root spreads and below-ground/above-ground allometries of plants in water-limited ecosystems. *J. Ecol.* 480–494.
- Schneider, C., Attinger, S., Delfs, J.O., Hildebrandt, A., 2010. Implementing small scale processes at the soil-plant interface—the role of root architectures for calculating root water uptake profiles. *Hydrol. Earth Syst. Sci.* 14, 279–289.
- Schnepf, A., Leitner, D., Landl, M., Lobet, G., Mai, T.H., Morandage, S., Sheng, C., Zörner, M., Vanderborght, J., Vereecken, H., 2018. Croobox: a structural-functional modelling framework for root systems. *Ann. Bot.* 121, 1033–1053.
- Schwinnig, S., Sala, O.E., 2004. Hierarchy of responses to resource pulses in arid and semi-arid ecosystems. *Oecologia* 141, 211–220.
- Shao, W., Ni, J., Leung, A.K., Su, Y., Ng, C.W.W., 2017. Analysis of plant root-induced preferential flow and pore-water pressure variation by a dual-permeability model. *Can. Geotech. J.* 54, 1537–1552.
- Simunek, J., Hopmans, J.W., 2009. Modeling compensated root water and nutrient uptake. *Ecol. Model.* 220, 505–521.
- Snyman, H., 2006. Root distribution with changes in distance and depth of two-year-old cactus pears *Opuntia ficus-indica* and *O. robusta* plants. *South Afr. J. Bot.* 72, 434–441.
- Somma, F., Hopmans, J., Clausnitzer, V., 1998. Transient three-dimensional modeling of soil water and solute transport with simultaneous root growth, root water and nutrient uptake. *Plant Soil* 202, 281–293.
- Song, L., Li, J., Zhou, T., Fredlund, D., 2017. Experimental study on unsaturated hydraulic properties of vegetated soil. *Ecol. Eng.* 103, 207–216.

- Stroosnijder, L., Moore, D., Alharbi, A., Argaman, E., Biazin, B., van den Elsen, E., 2012. Improving water use efficiency in drylands. *Curr. Opin. Environ. Sustain.* 4, 497–506.
- Taleisnik, E., Peyrano, G., Cordoba, A., Arias, C., 1999. Water retention capacity in root segments differing in the degree of exodermis development. *Ann. Bot.* 83, 19–27.
- Tardieu, F., 2012. Any trait or trait-related allele can confer drought tolerance: just design the right drought scenario. *J. Exp. Bot.* 63, 25–31.
- Tron, S., Bodner, G., Laio, F., Ridolfi, L., Leitner, D., 2015. Can diversity in root architecture explain plant water use efficiency? a modeling study. *Ecol. Model.* 312, 200–210.
- Uga, Y., Sugimoto, K., Ogawa, S., Rane, J., Ishitani, M., Hara, N., Kitomi, Y., Inukai, Y., Ono, K., Kanno, N., et al., 2013. Control of root system architecture by deeper rooting 1 increases rice yield under drought conditions. *Nat. Genet.* 45, 1097–1102.
- Van Genuchten, M.T., 1980. A closed-form equation for predicting the hydraulic conductivity of unsaturated soils 1. *Soil Sci. Soc. Am. J.* 44, 892–898.
- Van Genuchten, M.T., Pachepsky, Y.A., 2011. Hydraulic properties of unsaturated soils. *Encycl. Agrophysics* 368–376.
- Wesseling, J., 1991. Meerjarige simulaties van grondwateronttrekking voor verschillende bodemprofielen, grondwatertrappen en gewassen met het model swatre. *SC-DLO Rep.* 152, 40.
- Xu, S., Ji, X., Jin, B., Zhang, J., 2017. Root distribution of three dominant desert shrubs and their water uptake dynamics. *J. Plant Ecol.* 10, 780–790.
- Yamauchi, T., Colmer, T.D., Pedersen, O., Nakazono, M., 2018. Regulation of root traits for internal aeration and tolerance to soil waterlogging-flooding stress. *Plant Physiol.* 176, 1118–1130.
- Zhao, X., Xing, L., Shen, S., Liu, J., Zhang, D., 2020. Non-destructive 3d geometric modeling of maize root-stubble in-situ via x-ray computed tomography. *Int. J. Agric. Biol. Eng.* 13, 174–179.
- Zhu, J., Brown, K.M., Lynch, J.P., 2010. Root cortical aerenchyma improves the drought tolerance of maize (*Zea mays* L.). *Plant, Cell Environ.* 33, 740–749.